Journal of Materials Chemistry C

Accepted Manuscript

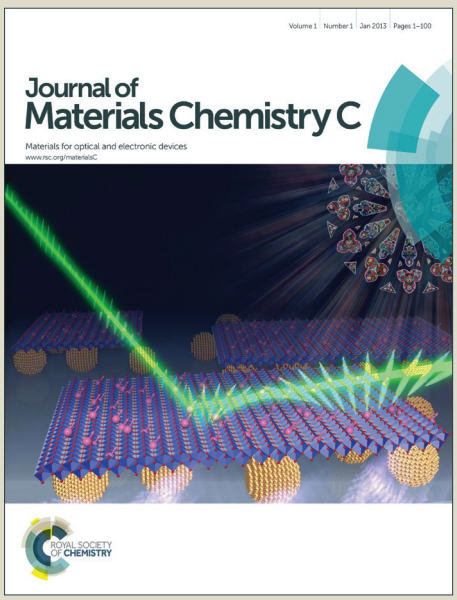

ROYAL SOCIETY OF CHEMISTRY

www.rsc.org/materialsC

Journal of Materials Chemistry C

ARTICLE

Broadband nonlinear optical and optical limiting effects of partially unzipped carbon nanotubes

Received 00th January 20xx,
Accepted 00th January 20xx

DOI: 10.1039/x0xx00000x

www.rsc.org/

Yan Zhang,[a] Yingpan Song,[a] Yao Gan,[a] Miao Feng,[a] and Hongbing Zhan*[a]

Many studies have shown that both carbon nanotubes (CNTs) and graphene are important broadband nonlinear optical (NLO) and optical limiting (OL) materials. As hybrid of CNTs and graphene, partially unzipped carbon nanotubes (PUCNTs) can be expected to exhibit superior NLO and OL effects. In this work, PUCNTs were obtained through lengthwise cutting and unraveling of multi-walled carbon nanotubes. The structure and component of PUCNTs were confirmed by transmission electron microscope, scanning electron microscopy, powder X-ray diffraction, Fourier-transform infrared and Raman spectra. NLO and OL properties were investigated by Z-scan technique at both 532 and 1064 nm in the nanosecond regime, in comparison with CNTs and graphene. Remarkable enhancement was observed, which can be attributed to the synergistic effect of nonlinear scattering and nonlinear absorption.

Introduction

Nonlinear optical (NLO) materials have received considerable attention in the past few decades because of their photonic and optoelectronic applications.[1-12] NLO materials can be optical limiting (OL) materials and saturable absorbers. OL materials exhibit decreased transmittance at high laser intensity, which can protect human eyes and delicate optical instruments from laser damage.[1-9] In contrast, the transmittance of saturable absorbers increases with the input laser intensity, which can be used for mode locking and Q-switching.[10-12]

Carbon nanotubes (CNTs) have been extensively studied for over two decades because of their remarkable electrical, thermal, optical and mechanical properties. Recently, it has been found that CNTs can be cut, or unzipped, lengthwise to form graphene nanoribbons.[13-17] By using oxidative opening technique, partially unzipped carbon nanotubes (PUCNTs) can be generated by adjusting the amount of oxidizing agent, oxidation time or temperature.[13,14] PUCNTs can be regarded as CNT–graphene hybrids with graphene like structure strongly attached to the intact inner walls of the nanotubes. They possess unique electronic and magnetic properties that are dependent on the degree of unzipping.[18] PUCNTs have shown promising applications in energy storage,[19] electrocatalysis[20] and electrochemical sensing.[21,22] However, despite the number of studies on the synthesis, electronic and electrochemical properties of PUCNTs, their optical and optoelectronic properties, especially NLO properties, remain largely unexplored.

Many studies have shown that both CNTs[23-26] and graphene [3,5,6,27-33] are important NLO and OL materials. While nonlinear scattering (NLS) is generally accepted as the principal mechanism for CNTs, NLS and nonlinear absorption (NLA) have been found both contribute to the NLO of graphene. As a hybrid between nanotubes and graphene,[33] we expect PUCNTs to form a new class of carbon-based nanostructures with superior NLO properties than either nanotubes or graphene.

In this paper, we prepared PUCNTs by longitudinal cutting and unravelling of multi-walled carbon nanotube (MWCNT) side walls. The NLO effects of PUCNTs are studied at both 532 and 1064 nm. As a control, the NLO effects of graphene oxide nanosheets (GNSs) and CNTs are also examined. The leading mechanisms for the NLO properties in PUCNTs are discussed.

Experimental section

Materials

MWCNTs (>97%, 20–40 nm in diameter and 5–15 μm in length) were purchased from Shenzhen Nanotech Port Co, Ltd, China. The other reagents were obtained from the Chinese Reagent Corporation and were of analysis grade. All the reagents were used as received without further purification.

Sample preparation

PUCNTs were obtained through lengthwise cutting and unraveling of the MWCNTs based on an optimized method presented by Tour et al.[13,14] $KMnO_4$ and concentrated H_2SO_4 were used as oxidizing agents. Briefly, MWCNTs (150 mg) were suspended in concentrated H_2SO_4 (36 mL), followed by ultrasonic treatment for 1 h. A second acid, H_3PO_4 (4 mL), was

[a]. College of Materials Science and Engineering, Fuzhou University, Fuzhou, Fujian, 350108, China. E-mail: hbzhan@fzu.edu.cn

added and the solution was treated by ultrasound for another 15 min. $KMnO_4$ (450 mg) was then added. The reaction mixture was heated to 45 ^{0}C and stirred for 2 h. The mixture was removed from the heat source and allowed to cool to room temperature. After the reaction was finished, the mixture was poured into 100 mL of ice water containing 5 mL of 30% H_2O_2. The resultant mixture was filtered on a 200 nm pore size polytetrafluoroethylene membrane, and then successively washed with HCl and deionized water until there was no SO_4^{2-} in the rinse water and the pH was neutral.

GNSs were synthesized by exfoliating oxidizing graphite powder using a modified Hummers method.[34] The graphite powder (5 g) was suspended in concentrated H_2SO_4 (110 mL) and H_3PO_4 (12 mL) by stirring for 1 h. $KMnO_4$ (15 g) was then slowly added, and the suspension was allowed to stir for another 2 h. The solution was heated to 38 ^{0}C for 0.5 h and then to 95 ^{0}C for 0.5 h. The mixture was poured into deionized water (220 mL) to terminate the reaction. A solution of 30% H_2O_2 (50 mL) was added dropwise and the mixture was then treated with gentle magnetic stirring for 15 min. The resultant mixture was filtered on a 200 nm pore size polytetrafluoroethylene membrane, and then successively washed with HCl and deionized water until there was no SO_4^{2-} in the rinse water and the pH was neutral. The yellow filter cake was re-suspended in deionized water. The mixture was treated with ultrasound and low speed centrifugation. The homogeneous and stable supernatant was dried using a freeze drier.

Characterizations

The microstructure characteristics of the CNTs and PUCNTs were investigated using a FEI Tecnai G2 F20 S-TWIN transmission electron microscope (TEM). The samples were dispersed in deionized water followed by mild ultrasonic treatment. A drop of the homogeneous solution was placed on a copper grid (3 mm diameter) and dried before being transferred to the TEM sample chamber. Surface morphologies and structures of the samples were observed by scanning electron microscopy (SEM) (Supra-55, Zeiss, Inc). Raman spectra were recorded using an Almega Raman spectrometer (inVia-reflex) at ambient temperature and using a 514.5 nm laser. Liquid samples suspended in deionized water were wiped clean directly before testing or being ground into powder. Powder X-ray diffraction (XRD) patterns were obtained with an XPert-PMD diffractometer, using Cu Kα radiation (λ=0.15405 nm, 40 kV, 100 mA). Fourier-transform infrared (FTIR) spectra were obtained using a Nicolet 5700 spectrometer. Spectrum was recorded from 4000 to 400 cm^{-1} using 12 scans at a resolution of 4 cm^{-1}. UV-Vis absorption spectra were detected using a Cary 50 spectrophotometer (UV-2450) and plotted in the wavelength range from 200 to 800 nm. Samples of suspensions were contained in 10 mm thick quartz cells.

NLO and OL measurements

The NLO and OL properties of the samples were investigated using an open-aperture Z-scan technique at wavelengths of 532 nm and 1064nm. The pulse of the Gaussian laser (250 uJ, 8 ns, 1 Hz) was from a Q-switched Nd:YAG laser. Through a 120 mm focal length lens, the laser beam radius was reduced to approximately 6 um. During the sample propagation along the Z-axis, the transmitting and scattering energy were obtained simultaneously, and were recorded by the detector behind the sample and the detector at an angular position of 45^o relative to the laser direction. The obtained data were further processed with a computer. All of the measurements were conducted at room temperature. CNTs, PUCNTs and GNSs suspensions were contained in 5 mm thick quartz cells. The linear transmittance (T_0) of all samples was adjusted to ~70% using a UV-Vis spectrometer.

Results and discussion

Material characterizations

Fig. 1 shows typical SEM and TEM images of PUCNTs and CNTs. From the SEM (Fig. 1(a) and (b)), it can be obviously seen that PUCNTs became wider after longitudinal unzipping; they stacked and entangled with each other due to the strong molecular interaction, and formed a three-dimensional structure on the substrate. CNTs (Fig. 1(c)) present a smooth, tubular structure with sharp edges. The diameters are between approximately 20–40 nm. They can be partially unzipped to give PUCNTs that are 100–120 nm wide and hundreds of nanometers long (Fig. 1(d)). The outer walls of the PUCNTs have developed a graphene–like structure, while the inner walls retain the hollow tubular structure of nanotubes.

Figure 1

Fig. 2(a) shows the XRD spectra of the samples. The CNTs' XRD spectrum shows a very strong characteristic peak at 26^o, corresponding to a *d* spacing. The peak can be attributed to the (002) planes of graphite and indicates a well-defined sp^2 structure with large domains.[13] The spectrum of PUCNTs shows that, as the reaction proceeds, the intensity of the peak at 26^o decreases and the peak gradually broadens. The decrease in the peak indicates increasing spacing, which result from the formation of oxygen moieties during the oxidation process.

Fig. 2(b) illustrates the FTIR spectra of the samples. Fig. 2(b) reveals the appearance of a C=O stretch at 1,700 cm^{-1} in PUCNTs. These C=O bonds from hydroxyl, carboxyl, carbonyl, and epoxy groups indicate that a large number of oxygen-containing groups exist on the PUCNTs.[13,14] The COO-H/O-H stretch (~3400 cm^{-1}) indicates the presence of carboxyl and hydroxyl functionalities as well as the possible presence of trapped water.

Fig. 2(c) shows the Raman spectra of the samples. There are two obvious main peaks for the CNTs. The Raman peak near 1342 cm^{-1} (D band) primarily originates from lattice defects,

such as vacancies, edge crimping, and sp^3-hybridized carbon atoms linked to the oxygen-containing groups. The peak near 1572 cm^{-1} (G band) is associated with sp^2-hybridized carbon atoms.[13,14] For the PUCNTs, the D band and G band appear at 1350 cm^{-1} and 1582 cm^{-1}, respectively. The ratios of I_D to I_G are 0.781 and 1.056 for CNTs and PUCNTs, respectively. The larger I_D to I_G ratio for the PUCNTs indicates a decrease in the sp^2/sp^3 ratio and an increasing level of disorder with increasing oxidation.

Figure 2

Fig. 3 gives the UV-Vis absorption spectra of the samples. GNSs have a maximum absorption at 230 nm, typical of the π-π* transitions of the aromatic C=C bonds. At around 300 nm, there is a shoulder which can be attributed to the n-π* transition of the C=O bonds.[35,36] The λ_{max} (254 nm) of CNTs, arises from π-π* transitions of sp^2 structure.[37] The absorption peak of PUCNTs exhibited a hypsochromic shift to 249 nm comparing to CNTs. With the longitudinal cutting and unravelling of CNTs, there is a decrease in π-π* transitions of sp^2 structure; the π-conjugated structure of PUCNTs is gradually destroyed. With the increase of SP^3 carbon atoms, the energy for the electron transfer process is increased, resulting in lower λ_{max}.[13,14]

Figure 3

NLO and OL properties analysis

Fig. 4 shows the typical open-aperture Z-scan results of the PUCNTs, GNSs, and CNTs. CNTs and GNSs were studied as a contrast to test the OL properties of PUCNTs. The measured open-aperture Z-scan curve can be fitted numerically to the transmission equation for a third-order nonlinear process, given by [38]

$$T = 1 - \beta I_0 L_{\text{eff}} / (\sqrt{8}(1 + z / z_0)^2) \quad (1)$$

Where T is the normalized transmittance, Z is the sample position, and I_0 is the on-axis irradiance at the focus. The effective thickness of the sample L_{eff} is given by $L_{eff} = [1 - \exp(-\alpha_0 l)]/\alpha_0$ (where l denotes thickness), $\alpha_0 = (-\ln T_0)/l$, α_0 is the linear absorption coefficient at a given wavelength, T_0 is the linear transmittance. $z_0 = k w_0^2/2$, and Z_O is the Rayleigh diffraction length. W_0 is the beam waist at z=0, which is the focal point. K=2π/λ, where k is the wave vector and λ is the laser wavelength. The calculated values of the nonlinear absorption coefficient (β_1) for GNSs, CNTs, and PUCNTs are shown in Table 1.

As shown in Fig. 4, all Z-scans exhibited a reduction in transmission around the focus of the lens, which indicates a broadband NLO response at both 532 and 1064 nm. PUCNTs exhibited excellent optical nonlinearity compared with CNTs and GNSs. At the focal point, the input fluence reached the maximum and the transmittance at 532 nm of GNSs, CNTs, and PUCNTs was reduced to a minimum (T_{min}) of 56.5, 31.8 and 25.7%, respectively (Fig. 4(a)). Therefore, PUCNTs demonstrate a superior NLO effect compared with GNSs and CNTs. Similarly, at 1064 nm, the T_{min} of GNSs, CNTs, and PUCNTs are 77.5, 61.2 and 58.0%, respectively (Fig. 4(b)), indicating that PUCNTs show the most prominent broadband NLO response. Obviously, the T_{min} at 532 nm are smaller than that at 1064 nm, which indicates that the NLO effect is much stronger at 532 nm compared with that at 1064 nm.

Figure 4

Fig. 5 shows the OL curves for GNSs, CNTs and PUCNTs at both 532 and 1064 nm. All of the samples exhibit a similar trend where in the transmittance remains constant at a low input fluence and then gradually decreases with an increasing input fluence at both 532 and 1064 nm, indicating a broadband OL effect. The OL threshold (F_{th}), defined as the input fluence at which the transmittance falls to half of the normalized linear transmittance, is summarized in Table 1. It can be seen that PUCNTs show a much lower F_{th} than GNSs and CNTs at both 532 and 1064 nm. Besides, the F_{th} value of the PUCNTs is much lower than recently reported other oxygenated carbon nanomaterials,[39, 40] suggesting the superior OL property of PUCNTs.

Figure 5

The broadband NLO effect observed from PUCNTs can be principally attributed to NLS. The NLS curves are shown in Fig. 6. The normalized transmittance T is related to the sample position Z by equation (1). The calculated values of the nonlinear scattering coefficient (β_2) for GNSs, CNTs, and PUCNTs are shown in Table1.[38] For the PUCNTs, there is a significant scattering peak that is symmetric with respect to the focus, indicating a strong NLS effect. The scattering intensity in PUCNTs is stronger than that in GNSs and CNTs at both 532 and 1064 nm. This occurs for the following two reasons. First, according to the Mie scattering theory,[3,27,41-43] effective scattering arises from the formation of scattering centers whose sizes are comparable to the wavelength of the incident laser beam.[3,29,42,44] Nonlinear scattering centers arising from the formation of solvent bubbles and microplasmas is the dominating mechanism for optical limiting.[26,45,46] We deduce that the differently sized GNSs, CNTs, and PUCNTs may lead to different-sized scattering centers. The size of PUCNTs is between GNSs and CNTs, and the size of the scattering centers formed in PUCNTs may be closest to the wavelength of the incident laser, which will generate the strongest scattering intensity. Second, many of the previously reported NLO studies of graphene-based nanocarbon suspensions have revealed that induced thermal scattering is the principle mechanism contributing to the observed OL.[45] Nanoparticles are heated up and transfer the heat energy to the surrounding solvent during intense laser pulses. This localized heating generates the formation of solvent bubbles, which expand quickly because of the large pressure difference at the vapor–solution

interface.[3] The PUCNTs exhibit a larger thermal conductivity in water than CNTs and GNSs. Meanwhile, the scattering intensities of all of the samples are weaker at 1064 than at 532 nm, consistent with the trend of the NLO behavior of the samples.

Figure 6

In addition to NLS, it is notable that NLA may play an important role in the NLO effect.[47-50] NLA can be divided into excited-state absorption (ESA), two-photon absorption (TPA), and multi-photon absorption (MPA).[30] For graphene oxide materials, ESA dominates the NLA process during nanosecond pulses, while TPA/MPA plays an important role in the case of picosecond pulses.[51] Therefore, as hybrid of nanotubes and graphene, the graphene-like structure in PUCNTs can generate NLA. PUCNTs have a structure of sp^3-hybridized carbon atoms linked to oxygen-containing groups and sp^2-hybridized carbon atoms. The stronger NLA of PUCNTs results from the combination of TPA from sp^3-hybridized domains and reverse saturable absorption (RSA) in sp^2 domains.[52] Additionally, investigations have shown that large sp^2 domains tend to induce SA, while small sp^2 domains separated by sp^3 hybridized carbon atoms are prone to induce NLA in graphene materials.[53-57] Research regarding some reduced GO films, with various degrees of reduction, has shown that the OL achieved increases with increasing ratio of sp^2/sp^3 domains.[29,53] As a result of oxidation reactions, PUCNTs have more sp^3 clusters than CNTs and GNSs. Compared with GNSs and CNTs, the narrower graphene-like structure in PUCNTs generates more small-sized localized sp^2 domains, which decreases the rate of non-radiative recombination and allows stronger NLA.

Table 1

Conclusions

PUCNTs are formed by lengthwise cutting and unravelling of CNTs. The outer walls of the CNTs have been cut to form graphene–like structures with different sizes, while the inner walls retain the hollow tubular structure of nanotubes. These observations were confirmed by SEM and TEM analysis. XRD, FTIR, and Raman spectra revealed that PUCNTs have a structure of sp^3-hybridized carbon atoms linked to oxygen-containing groups and sp^2-hybridized carbon atoms. Larger NLO and OL properties were discovered for the PUCNTs compared with those of GNSs and CNTs. PUCNTs show a much lower F_{th} than GNSs and CNTs at both 532 and 1064 nm, indicating a remarkable broadband OL effect. This can be attributed to their stronger NLS and NLA. The size of scattering centers and larger thermal conductivity of PUCNTs is deduced to result in stronger NLS. Meanwhile, the stronger NLA of PUCNTs is due to an increase number of localized sp^2 domains and the combination of TPA and RSA. The NLO and OL effects were enhanced at both 532 and 1064 nm, which indicates that PUCNTs are promising candidates for practical broadband optical limiters.

Acknowledgements

This research was supported by the National Natural Science Foundation of China (Nos. 51172045 and 51402051)

Notes and references

1 J. W. Perry, K. Mansour, I. Y. S. Lee, X. L. Wu, P. V. Bedworth, C. T. Chen, D. Ng, S. R. Marder, P. Miles, T. Wada, M. Tian and H. Sasabe, *Science*, 1996, **273**, 1533-1536.
2 Y. Chen, M. Hanack, Y. Araki and O. Ito, *Chem. Soc. Rev.*, 2005, **34**, 517-529.
3 J. Wang, Y. Hernandez, M. Lotya, J. N. Coleman and W. J. Blau, *Adv. Mater.*, 2009, **21**, 2430-2435.
4 G. Zhou, W. Wong, Chem. Soc. Rev., 2011, **40**, 2541-2566.
5 G. K. Lim, Z. Chen, J. Clark, R. G. S. Goh, W. H. Ng, H. Tan, R.H. Friend, P. H. K. Hoand and L. L. Chua, *Nat. Photon.*, 2011, **5**, 554-560.
6 Y. Xu, Z. Liu, X. Zhang, Y. Wang, J. Tian, Y. Huang , Y. Ma , X. Zhang and Y. Chen, *Adv. Mater.*, 2009, **21**, 1275-1279.
7 S. Hirata, K. Totani, T. Yamashita, C. Adachi and M. Vacha, *Nat. Mater.*, 2014, **13**,938-946.
8 G. Zhou, W. Wong, *Chem. Soc. Rev.*, 2011, **40**, 2541-2566.
9 G. Zhou, W. Wong, C. Ye, Z. Lin, *Adv. Funct. Mater.*, 2007, **17**, 963-975.
10 K. Wang, J. Wang, J. Fan, M. Lotya, A. O'Neill, D. Fox, Y. Feng, X. Zhang, B. Jiang, Q. Zhao, H. Zhang, J. N. Coleman, L. Zhang and W. J. Blau, *ACS Nano*, 2013, **7**, 9260-9267.
11 Q. L. Bao, H. Zhang, Y. Wang, Z. Ni, Y. Yan and Z. Shen, *Adv.Funct.Mater.*, 2009, **19**, 3077-3083.
12 W. B. Cho, J. H. Yim, S.Y. Choi, S. Lee, A. Schmidt, G. Steinmeyer, U. Griebner, V. Petrov, D. I. Yeom, K. Kim and F. Rotermund, *Adv. Funct. Mater.*, 2010, **20**, 1937-1943.
13 D.V. Kosynkin, A. L. Higginbotham, A. Sinitskii, J. R. Lomeda, A. Dimiev, B. K. Price and J. M. Tour, *Nature*, 2009, **458**, 872-876.
14 A. L. Higginbotham, D. V. Kosynkin, A. Sinitskii, Z. Sun and J. M. Tour. *ACS Nano*, 2010, **4**, 2059-2069.
15 L. Jiao, L. Zhang, L. Wang, G. Diankov and H. Dai. *Nature*, 2009, **458**, 877-880.
16 J. Wang, L. Ma, Q. Yuan, L. Zhu and F. Ding, *Angew. Chem. Int. Edit.*, 2011, **50**, 8041-8045.
17 D. B. Shinde, J. Debgupta, A. Kushwaha, M. Aslam and V. K. Pillai, *J. Am. Chem. Soc.*, 2011, **133**, 4168-4171.
18 B. Huang, Y. Son, G. Kim, W. Duan and J. Ihm, *J. Am. Chem. Soc.*, 2011, **131**, 17919-17925.
19 D. Yu, K. Goh, H. Wang, L. Wei, W. Jiang, Q. Zhang, L. Dai and Y. Chen, *Nat. Nanotechnol.*, 2014, **9**,555-562.
20 Y. Li, W. Zhou, H. Wang, L. Xie, Y. Liang , F. Wei, J. C. Idrobo, S. J. Pennycook and H. Dai, *Nat. Nanotechnol.*, 2012, **7**, 394-400.
21 Y. Song, M. Feng and H. Zhan. *Electrochem. Commun.*, 2014, **45**, 95-98.
22 H. Hu, M. Feng and H. Zhan, *Talanta*, 2015, **141**, 66-72.
23 J. Wang, D. Fruchtl, Z. Sun, J. N. Coleman and W. J. Blau, *J. Phys. Chem. C*, 2010,**114**, 6148-6156.
24 Z. Liu, J. Tian, Z. Guo, D. Ren, T. Du, J. Zheng and Y. Chen, *Adv. Mater.*, 2008, **20**,511-515.
25 S. Webster, M. Reyes-Reyes, X. Pedron, R. Lopez-Sandoval, M. Terrones and D. L. Carroll, *Adv. Mater.*, 2005, **17**, 1239-1243.
26 L. Vivien, P. Lancon, D. Riehl, F. Hache and E. Anglaret, *Carbon*, 2002, **40**, 1789-1797.
27 M. Feng, H. Zhan and Y. Chen, *Appl. Phys. Lett.*, 2010, **96**, 033107.
28 X. Jiang, L. Polavarapu, S. T. Neo, T. Venkatesan and Q. Xu , *J. Phys. Chem. Lett.*, 2012, **3**,785-790.

29 P. Chantharasupawong, R. Philip, N. T. Narayanan, P. M. Sudeep, A. Mathkar, P. M. Ajayan and J. Thomas, *J. Phys. Chem. C*, 2012, **116**, 25955-25961.
30 N. Liaros, P. Aloukos, A. Kolokithas-Ntoukas, A. Bakandritsos, T. Szabo, R. Zboril and S. Couris, *J. Phys. Chem. C*, 2013, **117**, 6842-6850.
31 Z. Sun, N. Dong, K. Xie, W. Xia, D. Konig, T. C. Nagaiah, M. D. Sanchez, P. Ebbinghaus, A. Erbe, X. Zhang, A. Ludwig, W. Schuhmann, J. Wang and M. Muhler, *J. Phys. Chem. C*, 2013, **117**,11811-11817.
32 N. Liaros, E. Koudoumas and S. Couris, *Appl. Phys. Lett.*, 2014, **104**, 1-5.
33 R.T. Lv, E. Cruz-Silva and M. Terrones, ACS Nano, 2014, 8, 4061-4069.
34 N. I. Kovtyukhova, P. J. Ollivier, B. R. Martin, T. E. Mallouk, S. A. Chizhik, E. V. Buzaneva and A. D. Gorchinskiy, *Chem. Mater.*, 1999, **11**, 771-778.
35 S. H. Aboutalebi, M. M. Gudarzi, Q. B. Zheng and J. Kim, *Adv. Funct. Mater.*, 2011, **21**, 2978–2988.
36 D. C. Marcano, D. V. Kosynkin, J. M. Berlin, A. Sinitskii, Z. Sun, A. Slesarev, L. B. Alemany, W. Lu and J. M. Tour, *ACS Nano*, 2010, **4**, 4806–4814.
37 I.S. Zaine , N.M. Napiah, A. M. Yusof, A.N. Alias, A. M. Ali, S.H. Khalid, *AMM.*, 2014, **661**, 8-13.
38 M. SheikBahae, A. A. Said, T. Wei, D. J. Hagan and E. W. VanStryland, *IEEE J. Quantum. Elect.*, 1990, **26**, 760–769.
39 X. Zhang, Z. Liu, X. Yan, X. Li, Y. Chen and J. Tian, *J. Optics-UK.*, 2015, **17**, 015501.
40 X. Zhang, Z. Liu, X. Zhao, W. Zhou and J. Tian, *Chem. Phys. Lett.*, 2010, **494**, 75-79.
41 J. Wang, W.J. Blau, *J. Opt. A-Pure Appl. Op.*, 2009, **11**,024001.
42 Y. Gan, M. Feng and H. Zhan, *Appl. Phys. Lett.*, 2014, **104**,171105.
43 Y. K. Dechizelle, S. L. Ceccio and C. E. Brennen, *J. Fluid. Mech.*, 1995, **293**, 99-126.
44 J. Wang, Y. Chen and W. J. Blau, *J. Mater. Chem.*, 2009, **19**, 7425-7443.
45 J. Wang, W. J. Blau, *Appl. Phys. B-Lasers O.*, 2008, **91**,521-524.
46 S. Sivaramakrishnan, V. S. Muthukumar, S.S. Sai, K. Venkataramaniah , J. Reppert, A.M. Rao, M. Anija, R. Philip and N. Kuthirummal, *Appl. Phys. Lett.*, 2007, **91**, 093104.
47 X. Zhang, Z. Liu, X. Li, Q. Ma, X. Chen, J. Tian, Y. Xu, and Y. Chen, *Opt. Express.*, 2013, **21**, 7511-7520.
48 H. Yang, X. Feng, Q. Wang, H. Huang, W. Chen, A.T.S. Wee and W. Ji, *Nano. Lett.*, 2011,**11**, 2622-2627.
49 S. Qu, Y. Zhang, H. Li, J. Qiu and C. Zhu, *Opt. Mat.*, 2006, **28**,259-265.
50 J. Venturini, E. Koudoumas, S. Couris, J. M. Janot, P. Seta, C. Mathis and S. Leach, *J. Mater. Chem.*, 2002, **12**, 2071-2076.
51 Z. Liu, Y. Wang, X. Zhang, Y. Xu, Y. Chen and J. Tian, *Appl. Phys. Lett.*, 2009, **94**, 021902.
52 Z. Liu, X. Zhao, X. Zhang, X. Yan, Y. Wu, Y. Chen and J. Tian, *J. Phys. Chem. Lett.*, 2011, **2**, 1972-1977
53 X. Zheng, M. Feng, Z. G. Li, Y. Song and H. Zhan, *J. Mater. Chem. C*, 2014, **2**, 4121-4125.
54 Z. Sun, N. Dong, K. Xie, W. Xia, D. Konig ,T.C. Nagaiah, M.D. Sanchez, P. Ebbinghaus, A. Erbe, X. Zhang, A. Ludwig, W. Schuhmann, J. Wang and M. Muhler, *J. Phys. Chem. C*, 2013, **117** ,11811-11817.
55 B. Anand, A. Kaniyoor,D. Swain, T. T. Baby, S.V. Rao, S.S.S. Sai, S. Ramaprabhu and R. Philip, *J. Phys. Chem. C*, 2014, **2**, 10116-10123.
56 X. Zheng, M. Feng and H. Zhan, *J. Mater. Chem. C*, 2013, **1**, 6759-6766.
57 G. Eda, Y. Y. Lin, C. Mattevi, H. Yamaguchi, H. A. Chen, I. Chen, C. Chen and M. Chhowalla, *Adv. Mater.*, 2010, **22**, 505–509.

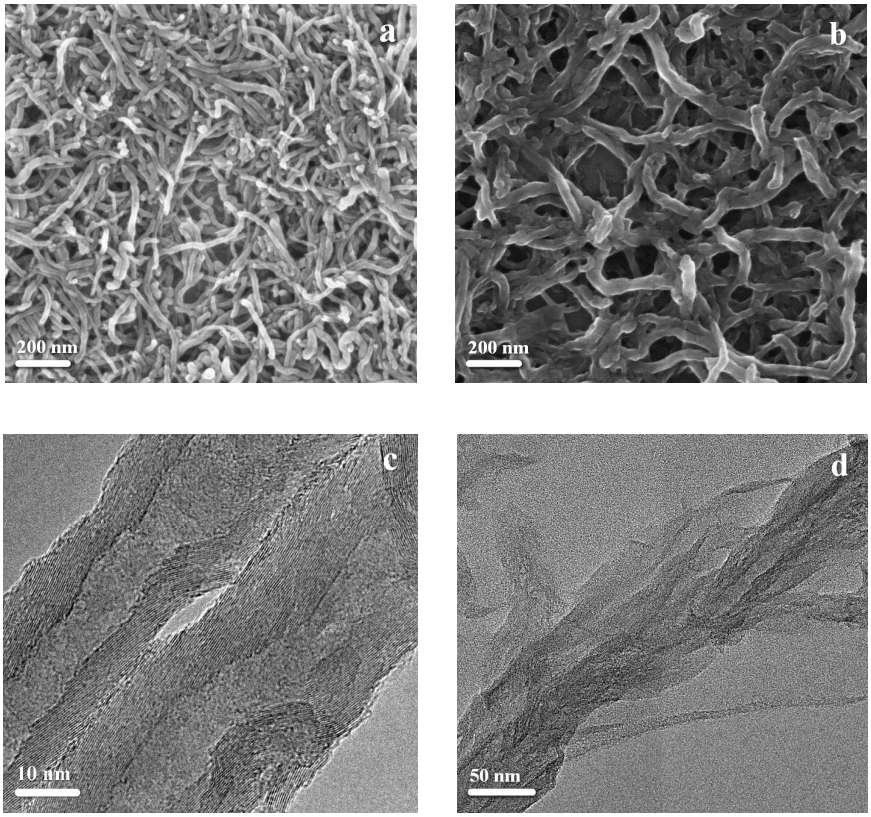

Figure 1. (a) SEM and (c) TEM images of CNTs; (b) SEM and (d) TEM images of PUCNTs.

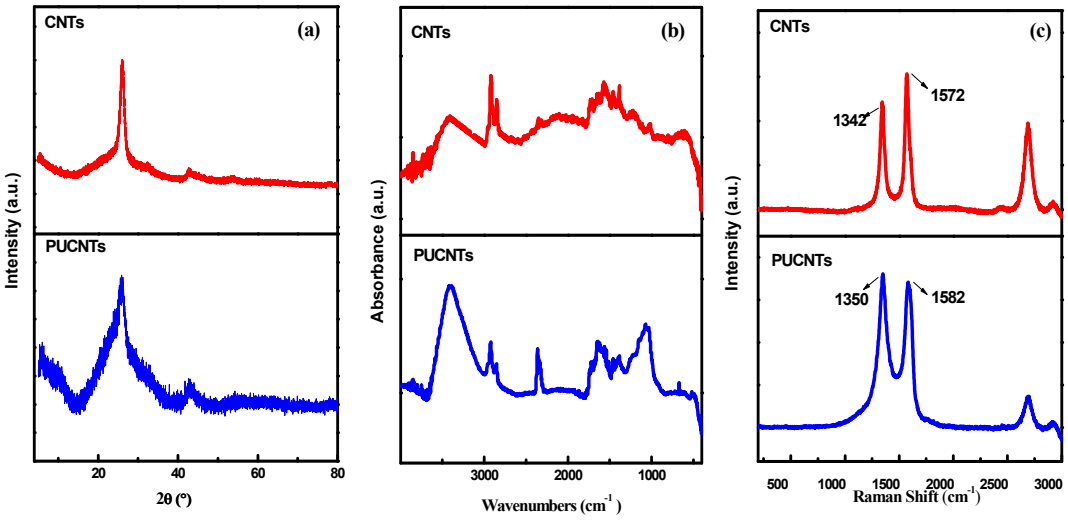

Figure 2. (a) XRD; (b) FTIR and (c) Raman spectra of CNTs and PUCNTs.

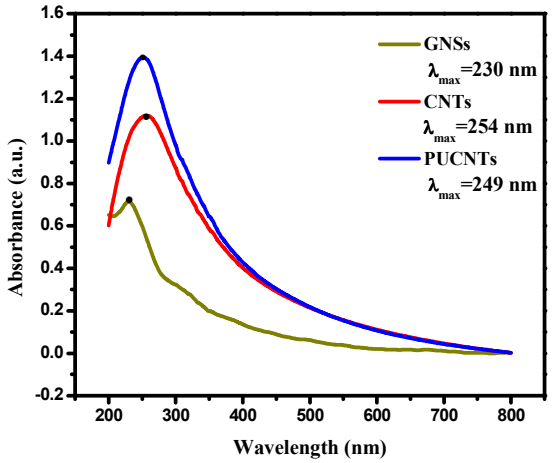

Figure 3. UV-Vis absorption spectra of GNSs, CNTs and PUCNTs

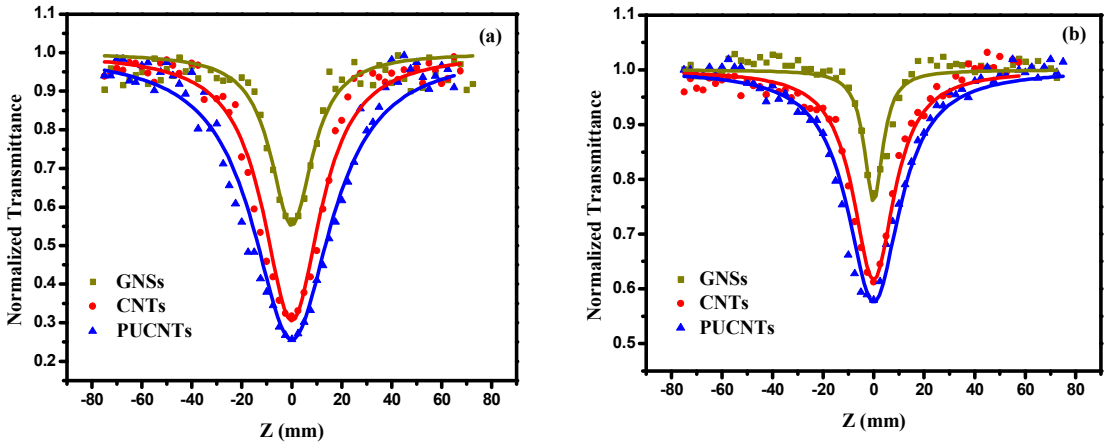

Figure 4. "Open-aperture" Z-scans results of GNSs, CNTs and PUCNTs under (a) 532 and (b) 1064 nm laser excitation.

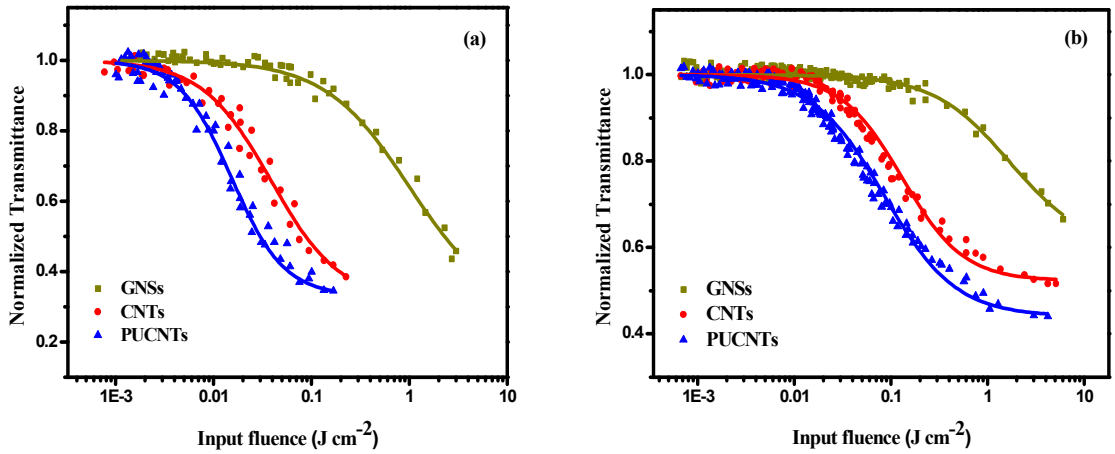

Figure 5. Variation of the normalized transmittance versus input fluence (J cm^{-2}) for GNSs, CNTs and PUCNTs at (a) 532 and (b) 1064 nm laser excitation.

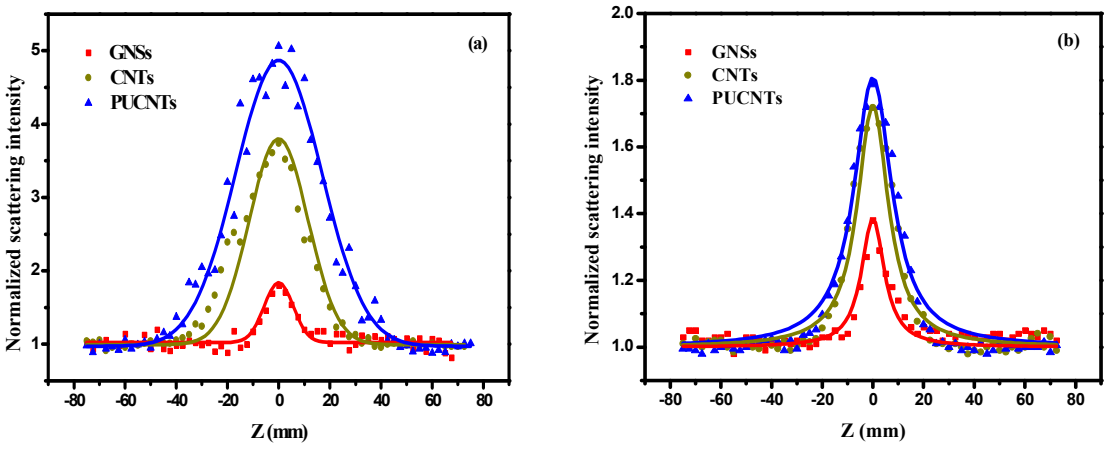

Figure 6. NLS results for GNSs, CNTs and PUCNTs at (a) 532 and (b) 1064 nm laser excitation.

Table 1. The NLA coefficient β_1, NLS coefficient β_2 (input energy of 250 μJ), and OL threshold (F_{th}) for samples at 532 and 1064 nm.

	532 nm			**1064 nm**		
Samples	$\beta_1\times10^{-10}$ (cm W^{-1})	$\beta_2\times10^{-9}$ (cm W^{-1})	F_{th} (J cm^{-2})	$\beta_1\times10^{-10}$ (cm W^{-1})	$\beta_2\times10^{-9}$ (cm W^{-1})	F_{th} (J cm^{-2})
GNSs	0.54	-0.11	2.3	0.29	-0.05	—
CNTs	0.82	-0.34	0.085	0.47	-0.08	>5
PUCNTs	0.91	-0.51	0.031	0.52	-0.09	0.52

Partially unzipped carbon nanotubes can be regarded as CNT–graphene hybrids with graphene like structure strongly attached to the intact inner walls of the nanotubes. They present a much lower F_{th} than graphene oxide nanosheets and carbon nanotubes at both 532 and 1064 nm, indicating a superior broadband optical limiting effect.